Available online at www.CivileJournal.org

Civil Engineering Journal

(E-ISSN: 2476-3055; ISSN: 2676-6957)

Vol. 12, No. 01, January, 2026

Theoretical Enhancement of Point Resistance in Sandy Soils Using Bio-Inspired Cranial Asperity Ratios

Agata Iwan Candra [1*], As'ad Munawir [1], Yulvi Zaika [1], Eko Andi Suryo [1]

[1] *Department of Civil Engineering, Brawijaya University, Malang 65145, Indonesia.*

Received 07 April 2025; Revised 15 November 2025; Accepted 04 December 2025; Published 01 January 2026

Abstract

This study aims to enhance the bearing capacity of pile foundations in sandy soils through a bio-inspired approach by modifying Meyerhof's empirical equation using a cranial correction factor. The adjustment considers the geometric influence of the asperity length–height ratio (L/H 20, 26.67, and 33.33) applied to different pile diameters. The analysis was carried out theoretically by calculating point resistance (Qp) using the modified equation, followed by validation through ANOVA and the nonparametric Mann–Whitney test. The results indicate that an L/H ratio of 20 provides the most significant improvement in Qp, ranging from 11.7% to 465.8% compared to the conventional Meyerhof model, particularly at lower D/B ratios where stress concentration can be optimally mobilized. Larger ratios such as 26.67 and 33.33 also improve capacity, though less effectively than L/H 20, yet still outperform unmodified foundations. The correction factors obtained, ranging from C_r 1.07 to 5.66, demonstrate the substantial contribution of geometric modification to load transfer efficiency. The novelty of this research lies in integrating anisotropic interface properties into the classical Meyerhof model, thereby bridging the gap between isotropic predictions and anisotropic experimental evidence. Accordingly, the developed theoretical framework not only strengthens the basis for calculating pile bearing capacity but also opens new avenues for bio-inspired foundation design that is more efficient and sustainable.

Keywords: Cranial Foundation; L/H Ratio; Modified Meyerhof Equation; Point Resistance; Load Transfer Efficiency.

1. Introduction

The optimization of pile foundation bearing capacity in sandy soils remains a pivotal challenge in contemporary geotechnical engineering [1, 2], owing to its critical role in ensuring structural stability and resource efficiency [3]. Classical empirical models, such as that proposed by Meyerhof, are extensively employed due to their simplicity; however, they inherently assume isotropic conditions at the soil–structure interface [4]. Consequently, the predicted tip and shaft resistances frequently underestimate the capacities observed in experimental investigations [5]. This discrepancy underscores the necessity for innovative approaches capable of more realistically capturing the mechanisms of soil–structure interaction, particularly by accounting for surface geometry, directional shear effects, and cyclic response under repeated loading, which are prevalent in practical foundation applications [6].

The phenomenon of anisotropic friction in snakes [7] has long attracted attention in biomechanics and tribology studies [8]. Snake locomotion exhibits a significant difference between cranial and caudal directions, with higher frictional resistance occurring during forward (cranial) movement [1]. Direct shear tests on ventral scales have demonstrated that cranial orientation can mobilize peak resistance up to 6.0 kPa and residual resistance of 9.1 kPa, whereas unidirectional cranial testing recorded an increase up to 22.0 kPa at a contact area of 0.21 [9]. This mechanism

* Corresponding author: agataiwan@student.ub.ac.id; iwan_candra@unik-kediri.ac.id

https://doi.org/10.28991/CEJ-2026-012-01-011

arises from the asymmetry of microstructural scales and serves as the fundamental inspiration for designing more efficient foundations through mechanical interlocking with soil grains [10, 11].

The application of directionally textured surfaces at the soil–structure interface has been proven to enhance load transfer [12]. Experimental studies have reported that bio-inspired piles can achieve a shaft friction ratio ranging from 2.98 to 16.36 in the cranial direction, substantially higher than that of rough steel piles, which is only about 4.0 [12]. Although this improvement is significant, technical drawbacks such as increased driving resistance and potential asperity wear remain as challenges for practical implementation [6]. In this context, load transfer efficiency is defined as the ability of foundations to transmit loads with minimal energy loss at the interface [10, 11]. Normalized roughness ratio (R_n) and asperity length-to-height ratio (L/H) serve as key parameters . Laboratory tests have shown that increasing Rn from 0.01 to 0.06 can raise the δ_{cs}/φ_{cs} ratio from 0.7 to 1.2, illustrating how minor changes in asperity geometry can yield considerable frictional gains [13]. Biomimetic studies based on the scales of *Leptophis ahaetulla* have identified an L/H ratio of approximately 20–33 as optimal for maximizing frictional anisotropy [14, 15].

Further experimental evidence substantiates this phenomenon, as a 10 mm pile with L/H 40 in Ottawa F65 sand was reported to exhibit a 780% increase in uplift capacity compared to a smooth pile [6]. At L/H 20, shaft capacity reached 6.3 MN at a depth of 11.6 m, representing an 845% improvement over the smooth pile [16]. Discrete Element Method (DEM) simulations with a 40 mm pile and L/H 18.75 demonstrated a 154% increase in axial capacity under cranial installation compared to caudal installation [17]. These findings confirm that asperities with smaller L/H ratios generate stronger soil interlocking, albeit with the consequence of higher installation resistance [18]. Moreover, cyclic loading studies revealed that anisotropically textured foundations are more capable of maintaining load-bearing capacity after multiple loading cycles, whereas smooth piles tend to degrade due to interface frictional loss. The cyclic tests indicated that cranial-oriented piles exhibited greater resistance. In dense sand at L/H 20, cranial capacity decreased from 0.90 to 0.37, while caudal capacity dropped from 0.42 to 0.18. At L/H 40, cranial piles still retained approximately 43% of their initial capacity [6].

The bearing capacity of pile foundations originates from the plastic behavior of materials under load, as described by Prandtl [19], and the application of differential equations by Reissner [20]. The ultimate soil bearing capacity (Q_u) is expressed as the sum of the pile's point resistance (Q_P) and skin resistance (Q_s) [21-23]. Key factors influencing this capacity include the pile size (A) [24], the depth of the loaded area (D), and the bearing capacity factor (N_q), which depends on the soil's internal friction angle. For various friction angles, N_q values range from 1 to 81.27 (0° - 40°) [25], 1 - 392,8 (0° - 50°), and 12,4 - 930 (20° - 45°) [4]. In the case of skin resistance (Q_s), the correction factor (K) adjusts for vertical soil stress [26, 27]. This factor was initially introduced by Meyerhof [28] and later refined by K researchers such as [28-30]. The soil's friction angle influencing typically falls within 33° to 43° [31], with specific studies reporting values as high as 38.5° [32-34].

Although these studies highlight the significant potential of bio-inspired approaches, classical empirical models such as Meyerhof [4] still assume isotropic conditions. As a result, the predicted point resistance (Q_P) tend to be lower than the outcomes observed in anisotropic experimental studies. This research gap remains unaddressed, as no analytical modification of Meyerhof's equation has yet incorporated anisotropy factors into the calculation of point resistance.

This study proposes a modification of Meyerhof's equation by introducing a Cranial Correction Factor (C_r), which represents the contribution of anisotropic friction from cranial asperities. The analysis was conducted on piles with diameters of 10 mm, 12 mm, and 15.85 mm, with L/H ratios of 20, 26.67, and 33.33. These ratios were selected as they correspond to the concave scale morphology of *Leptophis ahaetulla*, which has been shown to be the most efficient in generating frictional anisotropy. Theoretical validation was carried out using Analysis of Variance (ANOVA) to evaluate the significance of this parameter's influence on Qp at a 95% confidence level. The use of ANOVA is considered appropriate as an initial validation step prior to subsequent laboratory testing and numerical simulations.

The main contribution of this study lies in introducing a new dimension to the calculation of foundation bearing capacity by integrating anisotropic interface properties into the classical Meyerhof model. In doing so, the study bridges the gap between conventional isotropic models and anisotropic empirical evidence, while providing a theoretical framework with potential applications in the design of bio-inspired textured foundations. Accordingly, this research not only establishes a novel theoretical framework but also lays the groundwork for future experimental validation, making its outcomes relevant both academically and practically for bio-inspired foundation design.

The overall structure of this article is illustrated in Figure 1. It begins by introducing the background, motivation, and objectives that frame the research problem. This is followed by a presentation of the theoretical framework and the modified equations adopted to describe the load transfer mechanisms, which form the analytical foundation of the study. The paper then outlines the parametric configurations employed in the analysis, including variations in interface anisotropy and geometric ratios. Subsequently, the results derived from the theoretical models are discussed and interpreted in light of existing knowledge. Finally, the paper concludes by summarizing the main findings, highlighting limitations, and providing recommendations for future experimental validation.

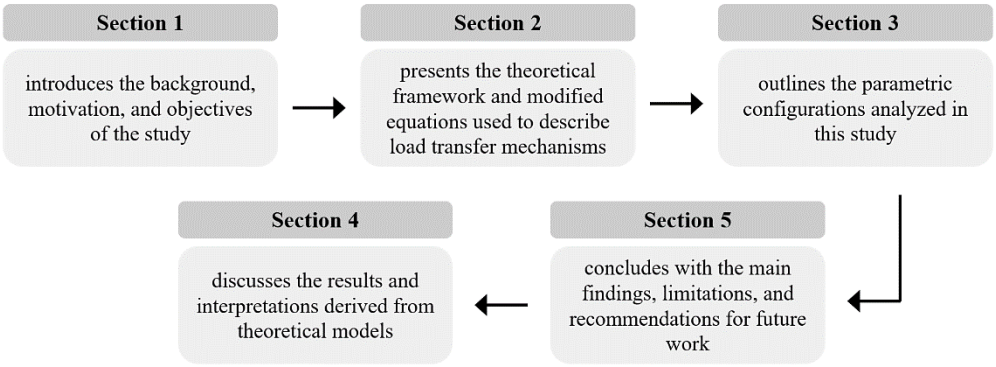

Figure 1. Structure Of This Article

2. Materials and Methods

The stages of this research are presented in Figure 2, where this study is entirely theoretical, building on Figure 3, which illustrates the geometric influence of the L/H ratio derived from cranial-inspired mechanisms. Using this basis, Meyerhof's empirical equation is modified to evaluate point resistance (Q_p) by incorporating soil properties such as friction angle (φ), and dry density (γ_t). The modification emphasizes the improvement in load transfer efficiency, demonstrating the critical role of asperity geometry in enhancing soil-structure interaction.

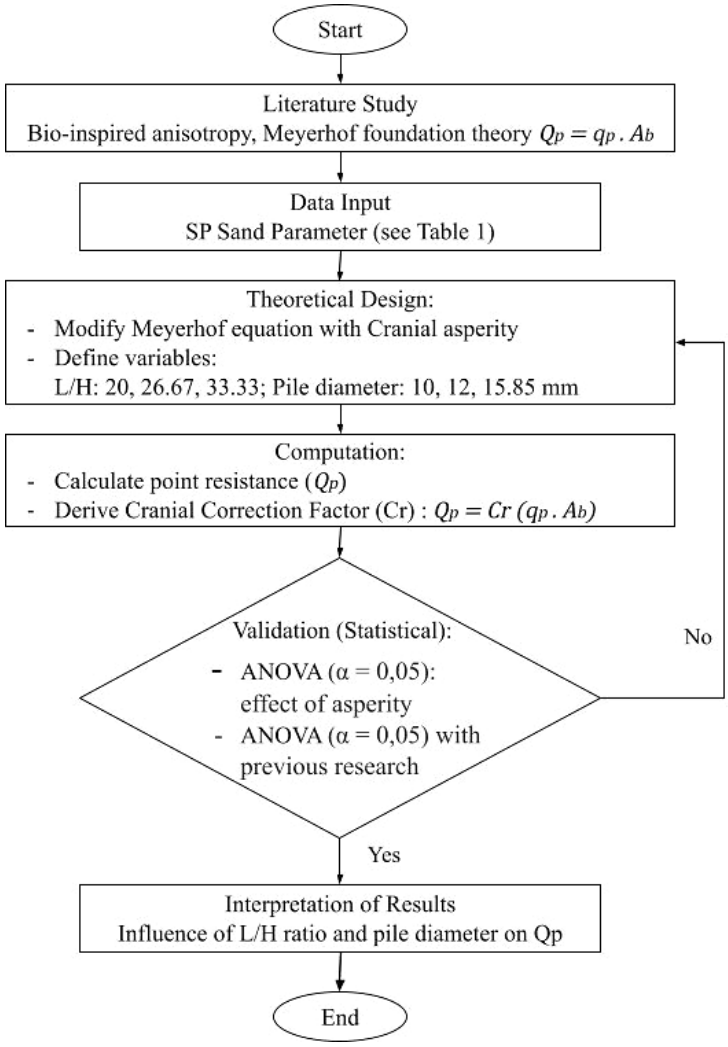

Figure 2. Flowchart of the Research

Three L/H ratios (20, 26.67, and 33.33) were prescribed to represent steep, moderate, and gentle asperity inclinations. The asperity height (H) was kept constant across configurations, while the asperity length (L) was varied to change L/H, enabling *an* isolated assessment of its effect on point resistance (Q_p). Figure 4 presents the schematic

representation of the piles used as the basis for theoretical calculations. Table 1 summarizes the soil properties applied in these calculations, which were incorporated into a modified equation to determine Q_p, values across different configurations.

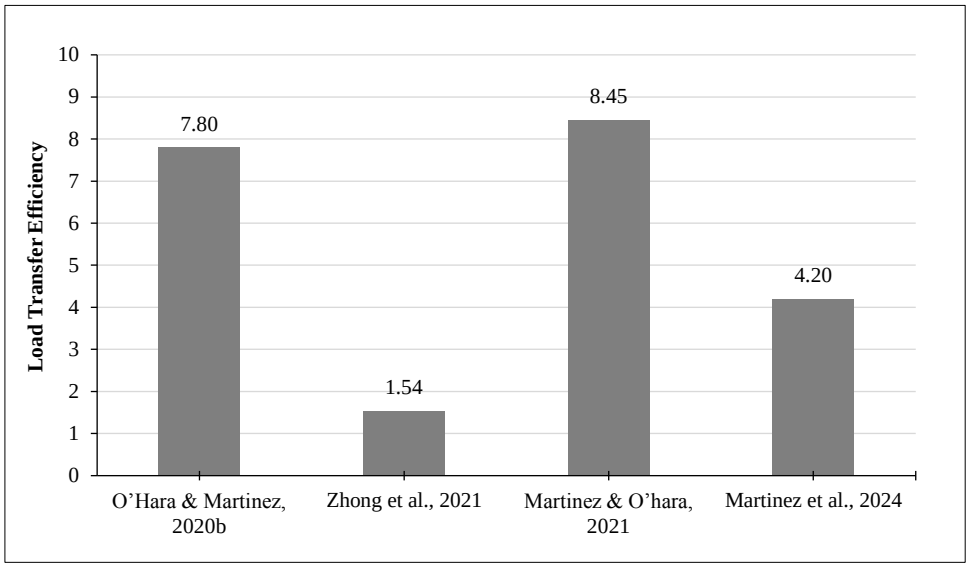

Figure 3. Basic Previous Research

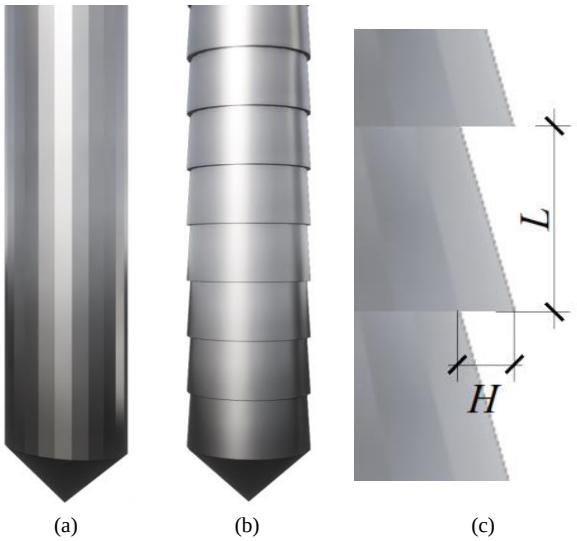

Figure 4. (a) Reference Foundation, (b) Cranial Foundation, (c) L/H Details

Table 1. Sand Properties

Properties	Value
Sand Type	SP
Dr (%)	70
Dry unit weight (γ_t) [kN/m³]	16.69
Uniformity coefficient Cu	3.42
Coefficient of curvature Cc	0.96
Average particle size D_{50} [mm]	0.40
Void ratio (e)	0.71
Maximum void ratio e_{max}	0.91
Minimum void ratio e_{min}	0.62
Porosity (%)	38.24
Specific Gravity (G_s)	2.76
Friction angle φ [°]	30

No load tests or numerical simulations using software were conducted. The results are derived solely from the theoretical application of the modified Meyerhof equation, ensuring a focus on mathematical relationships between soil properties, pile geometry, and the L/H ratio. In the context of foundation-point resistance [4], developed the point resistance equation (Q_p), which is generally expressed as follows:

$$Q_p = q_p \,.\, A_b \tag{1}$$

$$Q_p = \sigma` \,.\, N_q \,.\, A_b \tag{2}$$

where, point resistance (Q_p), bearing capacity of pile point (q_p), point surface area (A_b), Meyerhof bearing capacity factor (N_q), overburden effective stress (σ`).

Statistical validation of the theoretical calculations was conducted using Analysis of Variance (ANOVA). ANOVA was selected as it conforms to the data assumptions and effectively compares means across groups. However, non-parametric tests such as the Mann–Whitney test or sensitivity analysis can also be employed as complementary approaches to provide additional confidence in the results [35-37]. In this study, ANOVA was employed to assess the impact of the L/H ratio and pile diameter on the point resistance (Q_p). The F-statistic and p-values were computed to evaluate the significance of these parameters, with a significance level (α) set at 0.05. The analysis revealed statistically significant differences among the tested configurations, highlighting the critical role of geometric modifications in improving point resistance (Q_p) [38].

3. Results and Discussion

3.1. Results

Based on Figure 5, the inclusion of q_{pcr} in the L/H profile of cranial foundations necessitates modifications to Meyerhof's original equations (Equations 1 and 2). These adjustments result in equations (Equations 3 and 4), which refine the calculated Q_p values. The presence of q_{pcr} along the shaft of the pile significantly influences the overall Q_p, as it alters the distribution of forces along the pile surface. Consequently, a correction factor is introduced to account for the L/H ratio specific to cranial foundations, modifying Meyerhof's equation for Q_p. The resulting equation, integrating the cranial correction, is derived as follows:

$$Q_{pcr} = Q_P + (q_{pcr} \,.\, A_{bcr} . N_{sb}) \tag{3}$$

$$Q_{pcr} = (q_p \,.\, A_b) + (q_{pcr} \,.\, A_{bcr} \,.\, N_{sb} \tag{4}$$

$$Q_{pcr} = (\sigma` \,.\, N_q \,.\, A_b) + (\sigma` \,.\, N_q \,.\, A_{bcr} . N_{sb} \tag{5}$$

$$Q_{pcr} = \left(\sigma` \,.\, N_q \,.\, \left(\tfrac{1}{4}\pi . B^2\right)\right) + \left(\sigma` \,.\, N_q \,.\, \left(\left(\tfrac{1}{4}\pi . B^2\right) - \left(\tfrac{1}{4}\pi . {B_{cr}}^2\right)\right) . N_{sb}\right) \tag{6}$$

$$C_r = \frac{\left(\sigma` .N_q .\left(\left(\frac{1}{4}\pi .B^2\right)-\left(\frac{1}{4}\pi .{B_{cr}}^2\right)\right).N_{sb}\right)}{\left(\sigma` .N_q .\left(\frac{1}{4}\pi .B^2\right)\right)} \tag{7}$$

$$C_r = \frac{Q_{pcr}}{Q_P} \tag{8}$$

The following terms are defined for the analysis: point resistance (Q_p), and cranial point resistance (Q_{pcr}), refer to the point load resistance at the pile tip, with cranial variations incorporating asperities at the pile interface. The point bearing capacity of the pile tip (q_p), and its cranial counterpart (q_{pcr}), represent the stress distribution at the pile point. Point surface area (A_b), and cranial point surface area (A_{bcr}), are calculated based on the pile geometry. Other parameters include pile diameter (B), Meyerhof bearing capacity factor (N_q), overburden effective stress (σ`), point total aspirities (N_{sb}), and cranial point resistance aspirities factor (C_r) which modifies the point resistance for cranial profiles.

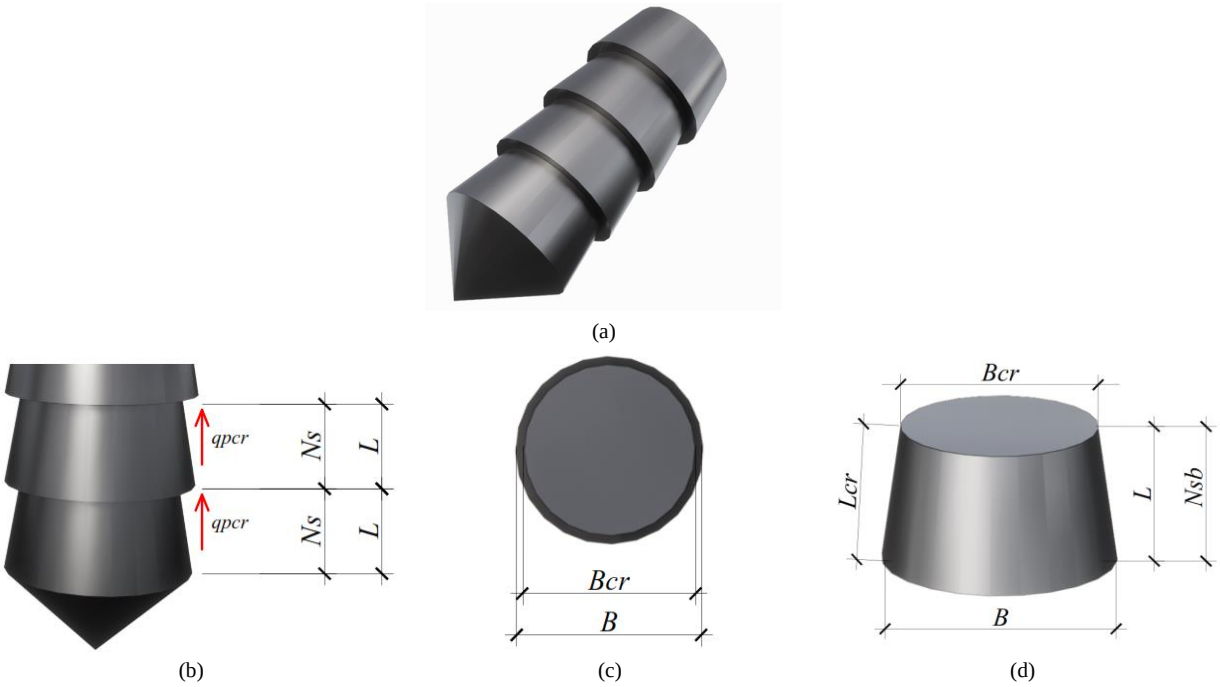

Figure 5. (a) 3D Detail of Cranial Foundations (b) Front View Detail of Cranial Foundations (c) Top View Detail of Cranial Foundations (d) Cross-section Detail of Cranial Foundations

3.1.1. Depth (D) vs Point Resistance (Q_p)

In Figure 6, all combinations of pile diameter (B = 10, 12, 15.85 mm) and asperity ratios (L/H = 20, 26.67, 33.33) demonstrate an increase in point resistance Q_p with increasing depth D in the range of 10–240 mm.

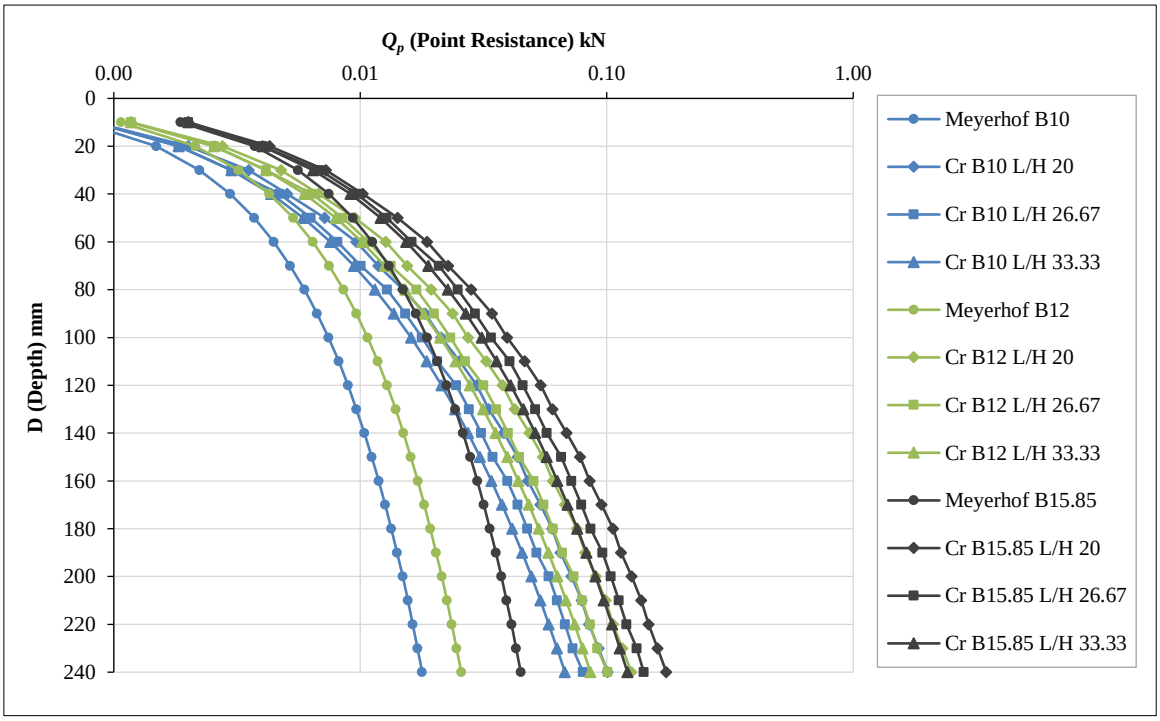

Figure 6. The Graph of the Depth (D) vs Point Resistance (Q_p)

In Figure 7, at a depth of D = 80 mm, the Meyerhof model with B = 15.85 mm produced Q_p= 0.015 kN; The cranial curve with B = 10 mm and L/H = 20 (L = 6) reached the same Q_p value, despite having a smaller diameter, with a difference of 5.85 mm or 36.9% relative to B = 15.85 mm. This finding indicates that cranial texturing can partially compensate for the reduced cross-sectional area of smaller piles by enhancing interface resistance. Consequently, pile geometry optimization through surface anisotropy may be as critical as increasing pile diameter in improving point resistance.

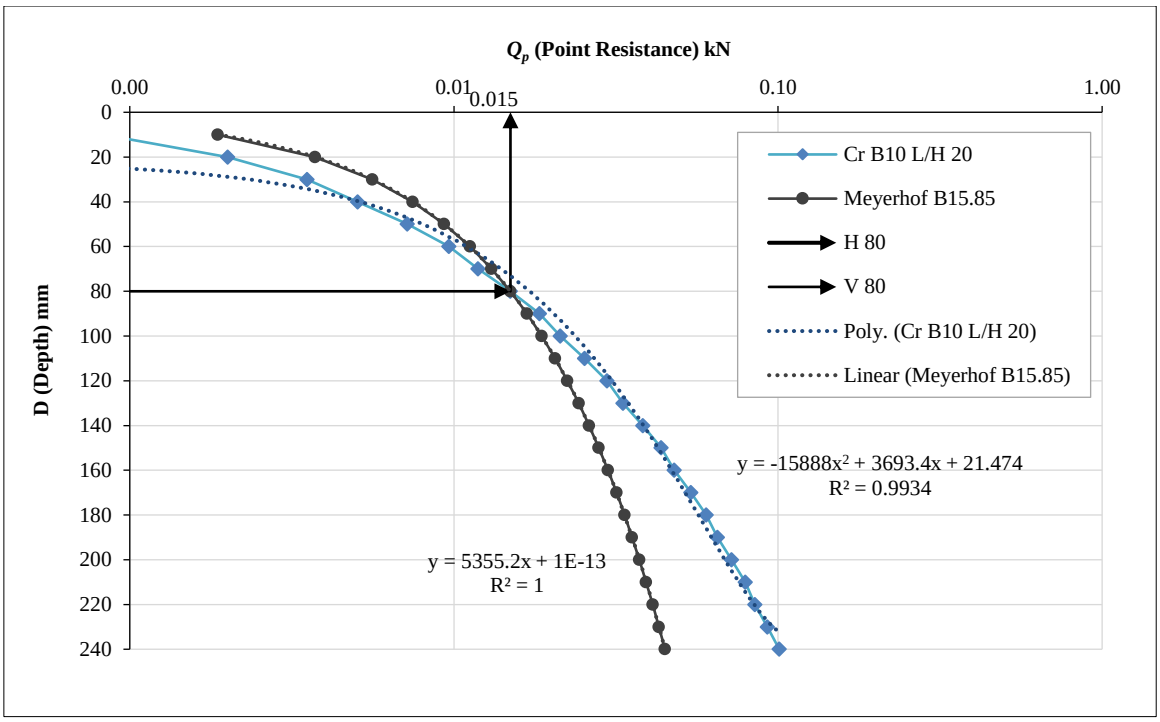

Figure 7. The Graph of the Relationship between Cranial B10 and Meyerhof B15.85

3.1.2. Depth/Diameter Ratio (D/B) vs Point Resistance (Q_p)

In Figure 8, Q_p is plotted against the depth–diameter ratio (D/B = 2–24) for all pile diameter combinations B (10, 12, 15.85 mm) and asperity ratios L/H (20, 26.67, 33.33). Figure 9 illustrates two intersection points yielding the same Q_p values at D/B = 6 between the Meyerhof model for B = 15.85 mm and the cranial configuration of B = 10 mm with L/H = 20; and at D/B = 14 between the Meyerhof model for B = 15.85 mm and B = 12 mm, L/H = 20. The regression equations obtained ($x = D/B$ and $y = Q_p$ in kN) are as follows: Meyerhof B = 15.85 mm, $y = -625.77x^2 + 224.72x + 1.9447$ ($R^2 = 0.9936$), cranial B = 12 mm, L/H = 20, $y = -1185.2\,x^2 + 336.85x + 2.4786$ ($R^2 = 0.9928$), and cranial B = 10 mm, L/H = 20, $y = 337.86x + 6 \times 10^{-15}$.

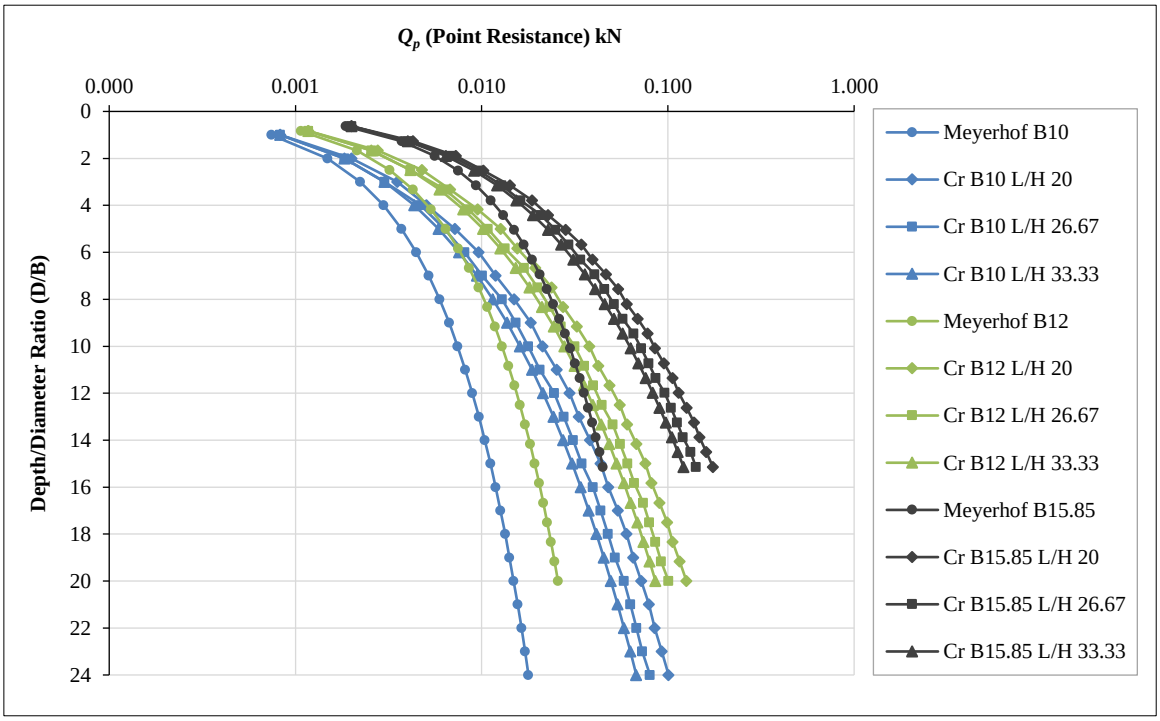

Figure 8. The Graph of the Relationship between Depth/Diameter Ratio (D/B) vs Point Resistance (Q_p)

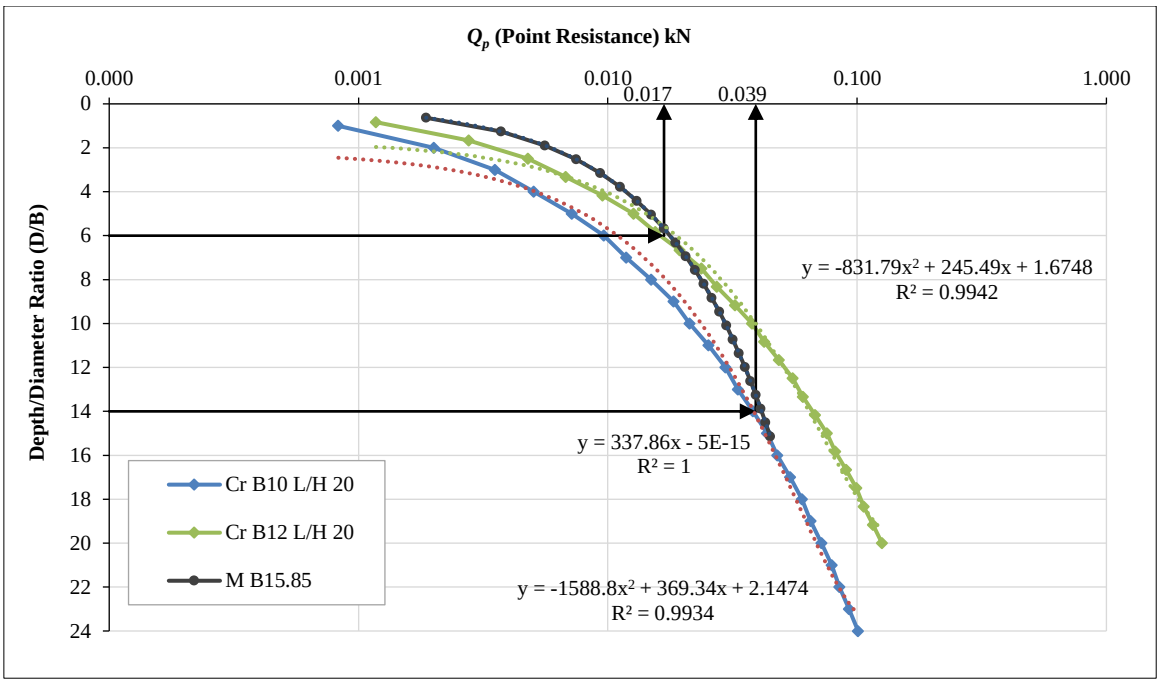

Figure 9. The Graph of the Relationship between Cranial B10 and Meyerhof B15

3.1.3. Depth/Diameter (D/B) vs Increase in Point Resistance (ΔQ_p)

In Figure 10, the increase in point resistance (ΔQ_p) is defined as $Q_{pcr} - Q_p$ and is plotted against the D/B ratio for all cranial configurations. At D/B = 14, the configuration with B = 10 mm and L/H = 20 yielded the lowest ΔQ_p value among the curves presented. At the same ratio, the curves for B = 10 mm, L/H = 20 and B = 12 mm, L/H = 26.67 were nearly coincident. The ΔQ_p (kN) axis scale in the graph was set at 0.005, 0.010, and 0.028.

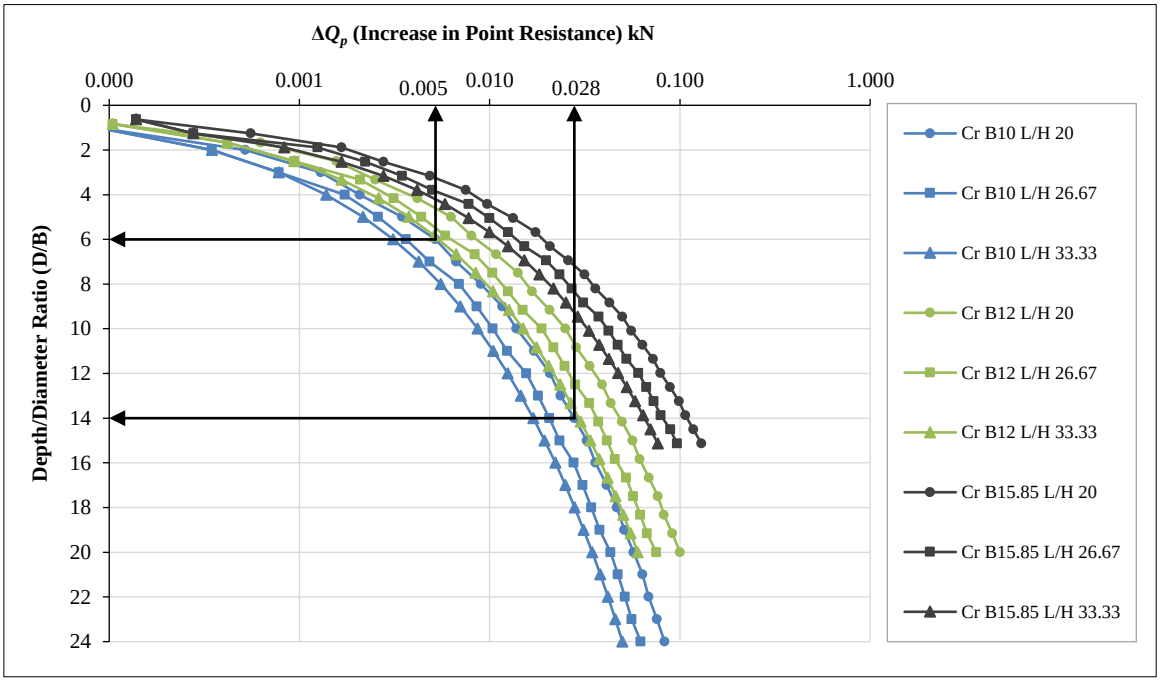

Figure 10. Graph Relationship between Depth/Diameter Ratio (D/B) vs Increase in Point Resistance (ΔQ_p)

3.1.4. Range of Q_p Enhancement Relative to Meyerhof

The range of Q_p enhancement (in percentage) relative to Meyerhof's predictions, as referenced from Figures 4 to 6 at depths of D = 10–240 mm, is summarized as follows. For L/H = 20, the configurations with B = 10, 12, and 15.85 mm exhibited increases of 11.7–465.8%, 9.7–390.0%, and 7.4–289.7%, respectively. At L/H = 26.67, the corresponding ranges were 11.7–349.4%, 9.7–292.5%, and 7.4–215.4% for B = 10, 12, and 15.85 mm. At L/H = 33.33, the values recorded were 11.7–279.5%, 9.7–234.0%, and 7.4–170.8% for the same diameters.

3.1.5. Meyerhof Equation Correlation

The theoretical results indicate that Meyerhof's equation for calculating the point resistance (Q_p) requires adjustments to account for the influence of the L/H ratio on cranial foundations. Based on the theoretical analysis presented in Table 1, the required modifications for each L/H ratio are as follows:

- L/H 20

$$Q_p = (1.07 - 5.66)\, q_p \,.\, A_b \tag{9}$$

At this ratio, the increase in Q_p ranges from 11.7% to 456.8% range for $B10$, 9.7% to 390% range for $B12$, and 7.4% to 289.7% range for $B15.85$ compared to the Meyerhof foundation at depths betwen 10 to 240 mm.

- L/H 26.67

$$Q_p = (1.07 - 4.49)\, q_p \,.\, A_b \tag{10}$$

For this ratio, the increase in Q_p ranges from 11.7% to 349.4% for $B10$, 9.7% to 292.5% range for $B12$, and 7.4% to 215.4% for $B15.85$ at depths between 10 to 240 mm. This indicates that the stress distribution and soil-pile interaction remain efficient, though slightly less optimal compared to L/H 20.

- L/H 33.33

$$Q_p = (1.07 - 3.79)\, q_p \,.\, A_b \tag{11}$$

At this ratio, the cap Q_p increase s only around 11.7% to 279.5% range for B10, 9.7% to 234.0% for B12, and 7.4% to 170.8% for B15.85 at depths between 10 to 240 mm.

3.1.6. Efficiency of Cranial Foundation Geometry

Cranial foundations with L/H 20 achieve a Q_p equivalent to Meyerhof foundations but with a diameter reduction of up to 58.5%. The cranial point resistance asperities factor (C_r), calculated as Q_{Pcr}/Q_P, quantifies the efficiency of capacity improvement due to asperity modifications. For diameters of 10, 12, and 15.85 mm, C_r values range from 1.07 to 5.66, indicating that higher values correspond to greater efficiency in enhancing bearing capacity

3.1.7. Statistical Validation

The ANOVA validation results in Table 2 confirm a statistically significant relationship between Q_p and Q_{pcr} at a significance level of α = 0.05. The F-Statistic values show variations among parameters $B10$, $B12$, and $B15.85$ across different L/H ratios. For instance, the highest F-Statistic value 20.27 is observed for $B10$ with L/H 20, while the lowest value 10.87 occurs for $B15.85$ with L/H = 33.33. Additionally, all P-Values in the table are smaller than α = 0.05. For example, for $B10$ with L/H = 20 has a P-Value is $4.58\text{x}10^{-5}$, while $B15.85$ with L/H = 33.33 has a P-Value is $1.89\text{x}10^{-3}$. These findings confirm that the relationship between Q_p and q_{pcr} is significant at a 95% confidence level. The decreasing F-Statistic values with increasing L/H suggest that the L/H ratio influences the strength of this relationship.

Table 2. Validation of ANOVA Q_p with Q_{pcr}

Parameters	B10 (L/H)			B12 (L/H)			B15.85 (L/H)		
	20	26.67	33.33	20	26.67	33.33	20	26.67	33.33
F-statistic	20.27	17.80	16.14	18.85	16.21	14.43	15.79	13.03	10.87
P-Value	4.58×10^{-5}	1.14×10^{-4}	2.16×10^{-4}	7.69×10^{-5}	2.10×10^{-4}	4.25×10^{-4}	2.47×10^{-4}	7.53×10^{-4}	1.89×10^{-3}

3.1.8. Comparison with Previous Studies

The Statistical analysis, referring to Table 3, was conducted to compare the C_r values from theoretical calculations (for diameters of 15.85 mm, 12 mm, and 10 mm) with data from studies [16, 39-42]. The data from these previous studies were extracted from Figure 3 for consistency and accuracy in comparison. The ANOVA test in Table 3 shows an *F-statistic* value of 2.305 with a *P-value* of 0.167 ($P > 0.05$). Nonparametric validation using the *Mann–Whitney* test yielded a *P-value* of 0.166 ($P > 0.05$). The consistency of these two methods confirms that there are no significant differences between the theoretical results and the previous study data.

Table 3. Statistical Analysis of C_r Previous Research and This Research

ANOVA (One-Way)		Nonparametric (Mann-Whitney)
F	P-value	P-value
2.305	0.167	0.166

The theoretical model used in this study has proven capable of accurately representing load transfer efficiency across various pile diameters and asperity configurations. Although some maximum values reported in studies [6, 12, 40] are slightly higher, the theoretical results remain within a relevant range. Therefore, as supported by the analysis in Table 3 and the data in Figure 1, this theoretical approach is valid for describing the load transfer mechanism in pile foundations.

3.2. Discussion

3.2.1. Q_p and ΔQ_p in Relation to D and D/B

In Figure 6, the point resistance (Q_p) increases with depth (D) across all combinations of pile diameter (B) and asperity ratio (L/H). At D = 80 mm, the Q_p value predicted by the Meyerhof model for B = 15.85 mm coincides with that of the cranial configuration B = 10 mm, L/H = 20 (Figure 7). In the non-dimensional domain, the Q_p versus D/B plot exhibits the highest values at D/B ≤ 24, whereas for D/B ≥ 30 the rate of increase becomes less pronounced (Figure 8). Curve intersections at D/B = 6 and 14 illustrate configuration pairs producing identical Q_p values (Figure 7). The $\Delta Q_p = Q_{pcr} - Q_p$ plotted against D/B reveals the convergence of responses among certain cranial configurations; for example, at D/B = 14, the curve for B = 10 mm, L/H = 20 nearly coincides with that of B = 12 mm, L/H = 26.67 (Figure 10). These findings indicate that asperity effects are more dominant at lower D/B ratios, whereas at higher ratios the influence of geometry tends to diminish due to the wider distribution of stresses along the contact area.

3.2.2. Evaluation of Theoretical Model Accuracy

The validity of the theoretical predictions is supported by strict control of variables, where the sand material and boundary conditions were kept identical, as well as by the consistency of responses across pile diameters (B = 10–15.85 mm). This is consistent with the design of directional interface tests on snake-scale-inspired surfaces and anisotropic interfaces [43, 44].

Statistical verification was performed using one-way ANOVA, where all comparisons in Table 2 yielded $p < 0.05$, while external comparisons in Table 3 reported F = 2.305 with p = 0.167. This analysis was further validated through the non-parametric Mann–Whitney test, which yielded P = 0.166 (P > 0.05). The consistency between parametric and non-parametric outcomes confirms that no significant differences exist between the theoretical results and previous research data, thereby reinforcing the reliability of the quantitative evaluation approach for interface parameters, as commonly adopted in sand–steel friction studies [45].

Moreover, the tendency for capacity to increase at greater depths is consistent—as a mechanistic inference—with findings that anisotropic friction modifies stress distribution and redistribution while enhancing resistance mobilization, even in dilatant sands [43, 46, 47]. Meanwhile, increasingly dominant interlocking has been shown to improve interface shear capacity on rougher surfaces and with more angular particle geometries [45].

3.2.3. Critical Parameters: C_r, Asperities, and Load Transfer Efficiency

The cranial correction factor (C_r) is dimensionless and represents the efficiency of end resistance (Q_p) enhancement due to the application of cranial asperities at the pile–soil interface. The anisotropic texturing effect, which increases interface shear resistance, has been demonstrated in studies of snake scale–inspired surfaces as well as sawtooth interfaces. A value of $C_r > 1$ indicates improvement over the Meyerhof baseline under the same soil conditions, whereas $C_r = 1$ denotes no change.

Asperities are defined by the parameters L (asperity length) and H (asperity height), which determine the shape and inclination of the profile and directly influence interface shear behavior. In this study, L/H ratios of 20, 26.67, and 33.33 were selected as they represent slope variations commonly observed in reptile scale patterns [44] and align with prior recommendations emphasizing the need for geometrical contrasts that remain realistic in terms of manufacturability [43]. Thus, the parameter selection is supported by both biological relevance and existing literature.

Load transfer efficiency is defined as the relative improvement in tip capacity over the Meyerhof baseline under identical soil conditions and boundaries, directly reflected by the C_r value. The increase in efficiency is consistent with experimental evidence showing that surface texturing patterns significantly enhance the shear strength of sand–steel interfaces.

3.2.4. Installation Challenges and Constructability

Micro-texturing on the pile shaft has the potential to increase installation resistance during driving, while simultaneously inducing asperity wear and requiring high geometric precision. To mitigate these adverse effects, the use of wear-resistant materials, chamfering or rounding of asperity tips, modular processing through prefabrication or precision machining, and installation methods that preserve texture integrity are recommended.

Such practices are consistent with the bio-inspired approach, which emphasizes the importance of precision manufacturing in maintaining the functional performance of micro-textures. Similar observations were reported [43], who highlighted that quality control in techniques such as laser texturing and additive manufacturing is a key factor in ensuring the effectiveness of textures in terms of tribological function and mechanical durability [41].

3.2.5. Geometric Scale Effects

Within the diameter range of B = 10, 12, and 15.85 mm, the absolute Q_p value increases with B ($Ab \propto B^2$), yet the relative efficiency C_r remains nearly constant across diameters (Figures 8–10). This indicates that geometric ratios such as L/H are the primary controlling factors. Application of the results to larger diameters requires maintaining relative roughness ($H/D_{50}, L/D_{50}$) to ensure consistency of interaction mechanisms. Recent studies have reported that pile tip resistance in very dense sand increases with diameter, in accordance with the relationship $Ab \propto B^2$ [48, 49].

Other experimental and numerical findings have shown that particle interlocking significantly influences shear strength and dilation at peak conditions [50]. Moreover, DEM-based simulations indicate that geometric ratios affect overall shear strength and trigger the formation of shear banding, a narrow zone of high strain where granular material failure occurs [51]. Until further verification becomes available, the use of C_r values is recommended conservatively within the experimental range obtained.

3.2.6. Position Within Recent Modifications

Compared to conventional approaches such as helical and under-reamed foundations, which enhance bearing capacity through macro-geometric alterations and installation effects, as well as tapered or cone-top piles that regulate stress distribution by geometric shaping, the snake-skin textured surface proposed in this study offers a distinct working mechanism. This design optimizes pile tip contribution through anisotropic microstructures that are materially efficient and can be readily integrated into the classical Meyerhof bearing capacity formulation via a single modification parameter (C_r). Other bio-inspired approaches, such as root-type foundations, have also demonstrated performance gains through different strategies. Branched configurations of root-type piles increased uplift capacity by 30–50% in coral sand [52], while Huang & Martinez [53] showed that root-type anchor systems expanded the active shear zone and significantly enhanced lateral friction mobilization. In contrast, the snake-skin approach emphasizes soil–structure interaction improvement through controlled shear directionality and localized stress mobilization, as described by Martinez & O'hara [12] in their study on selective friction in textured piles. Therefore, this innovation occupies a distinctive position within the current landscape of foundation modifications, combining geometric efficiency, ease of integration into existing models, and biologically inspired surface mechanisms.

3.2.7. Practical Design Implications

Optimal performance zone is achieved at a diameter-to-width ratio (D/B) of up to 24 (Figures 8–10). Although data are not yet available for ratios above D/B > 24, there is no evidence of significant structural efficiency gains beyond this range. To ensure both structural and material efficiency, a length-to-height ratio (L/H) of 20 is recommended as the most favorable configuration.

Illustrations in Figures 7 and 9 demonstrate that a reduction in element diameter (e.g., from 15.85 mm to 10–12 mm) can be implemented without compromising tip resistance (Q_p), provided that the D/B ratio is maintained. This finding highlights significant opportunities for material savings and carbon footprint reduction. Such outcomes are consistent with the study of Zhang et al. [54], which emphasized the importance of geometric efficiency in sustainable engineering systems.

4. Conclusion

This study introduces a modification of Meyerhof's equation by incorporating a cranial correction factor (C_r) to account for the influence of the asperity length–height ratio (L/H) on the point resistance (Q_p) of pile foundations in sandy soils. The analysis shows that an L/H ratio of 20 represents the most optimal configuration, yielding increases in Q_p of 11.7–465.8% for a 10 mm diameter pile, 9.7–390.0% for a 12 mm pile, and 7.4–289.7% for a 15.85 mm pile at depths ranging from 10 to 240 mm. The most significant improvements occur at lower D/B ratios, where stress concentration can be maximized, allowing cranial geometry to partially substitute for larger pile diameters. These findings confirm that more uniform stress distribution and more efficient soil–pile interaction can be achieved through cranial-inspired geometric modifications. Larger L/H ratios, such as 26.67 and 33.33, still provide capacity improvements, though less effective than L/H = 20, yet consistently higher than foundations without cranial

modifications. The correction factors obtained—C_r = 1.07–5.66 (L/H = 20), C_r = 1.07–4.49 (L/H = 26.67), and C_r = 1.07–3.79 (L/H = 33.33)—quantitatively validate the efficiency of this design approach.

Theoretical validation using ANOVA confirmed statistically significant differences ($p < 0.05$) across configurations, while the Mann–Whitney test verified consistency with previous studies. These results indicate that the proposed model reliably describes load transfer in anisotropically textured foundations. From a practical perspective, cranial design offers potential material savings by reducing pile diameters up to 58.5% without compromising tip resistance, thereby improving efficiency and lowering the carbon footprint. However, as this study remains theoretical, further laboratory and field investigations are essential to validate the model and assess its performance under cyclic and long-term loading.

4.1. Limitations and Future Research

The model developed in this study has not yet been verified through field testing, does not account for the variability of soil properties, and does not incorporate material response under cyclic or dynamic loading. Accordingly, future research should include pile load tests in the field with varying L/H and ℓ/B ratios in asperity configurations to evaluate their contribution to load transfer efficiency, while also examining foundation system performance under diverse geotechnical conditions to assess sensitivity to soil heterogeneity. In addition, the development of nonlinear numerical models capable of realistically representing granular soil behavior is required, along with the evaluation of service life and asperity wear potential to ensure long-term performance sustainability. These recommendations are consistent with the bio-inspired approach, which emphasizes the importance of experimental validation and geometric optimization based on performance outcomes under complex and heterogeneous field conditions.

5. Declarations

5.1. Author Contributions

Conceptualization, A.I.C.; methodology, A.I.C.; software, A.I.C.; validation, A.I.C.; formal analysis, A.I.C.; investigation, A.I.C.; resources, A.I.C.; data curation, A.I.C.; writing—original draft preparation, A.I.C.; writing—review and editing, A.M., Y.Z., E.A.S; visualization, A.I.C.; supervision, A.M., Y.Z., E.A.S; project administration, A.I.C.; funding acquisition, A.I.C. All authors have read and agreed to the published version of the manuscript.

5.2. Data Availability Statement

The data presented in this study are available on request from the corresponding author.

5.3. Funding

The authors received no financial support for the research, authorship, and/or publication of this article.

5.4. Conflicts of Interest

The authors declare no conflict of interest.

6. References

[1] Gray, J., & Lissmann, H. W. (1950). The Kinetics of Locomotion of the Grass-Snake. Journal of Experimental Biology, 26(4), 354–367. doi:10.1242/jeb.26.4.354.

[2] Richards Jr, R., Elms, D. G., & Budhu, M. (1993). Seismic bearing capacity and settlements of foundations. Journal of Geotechnical Engineering, 119(4), 662-674. doi:10.1061/(ASCE)0733-9410(1993)119:4(662).

[3] Marvi, H., & Hu, D. L. (2012). Friction enhancement in concertina locomotion of snakes. Journal of the Royal Society Interface, 9(76), 3067–3080. doi:10.1098/rsif.2012.0132.

[4] Meyerhof, G. G. (1976). Bearing Capacity and Settlement of Pile Foundations. Journal of the Geotechnical Engineering Division, 102(3), 197–228. doi:10.1061/ajgeb6.0000243.

[5] Martinez, A., & Frost, J. D. (2017). The influence of surface roughness form on the strength of sand-structure interfaces. Geotechnique Letters, 7(1), 104–111. doi:10.1680/jgele.16.00169.

[6] O'Hara, K. B., & Martinez, A. (2020). Monotonic and Cyclic Frictional Resistance Directionality in Snakeskin-Inspired Surfaces and Piles. Journal of Geotechnical and Geoenvironmental Engineering, 146(11), 04020116. doi:10.1061/(asce)gt.1943-5606.0002368.

[7] Darwin, C. (1959). The Origin of Species, 1859-1959. Bios, 30(2), 67-72.

[8] DeJong, J. T., Burrall, M., Wilson, D. W., & Frost, J. D. (2017). A Bio-Inspired Perspective for Geotechnical Engineering Innovation. Geotechnical Frontiers 2017, 862–870. doi:10.1061/9780784480472.092.

[9] Martinez, A., & Palumbo, S. (2018). Anisotropic Shear Behavior of Soil-Structure Interfaces: Bio-Inspiration from Snake Skin. IFCEE 2018, 94–104. doi:10.1061/9780784481592.010.

[10] Mak, T. W., & Shu, L. H. (2004). Abstraction of biological analogies for design. CIRP Annals - Manufacturing Technology, 53(1), 117–120. doi:10.1016/S0007-8506(07)60658-1.

[11] Benz, M. J., Kovalev, A. E., & Gorb, S. N. (2012). Anisotropic frictional properties in snakes. Bioinspiration, Biomimetics, and Bioreplication 2012, 8339(i), 83390X. doi:10.1117/12.916972.

[12] Martinez, A., & O'hara, K. (2021). Skin friction directionality in monotonically-and cyclically-loaded bio-inspired piles in sand. DFI Journal, 15(1). doi:10.37308/DFIJnl.20200831.222.

[13] Han, F., Ganju, E., Salgado, R., & Prezzi, M. (2018). Effects of Interface Roughness, Particle Geometry, and Gradation on the Sand–Steel Interface Friction Angle. Journal of Geotechnical and Geoenvironmental Engineering, 144(12), 10–16. doi:10.1061/(asce)gt.1943-5606.0001990.

[14] Palumbo, S. (2018). Anisotropic Interface Shear Behavior of Granular Soil and Surfaces Biologically-Inspired by Snakeskin. Journal of Chemical Information and Modeling, 53(9), 1689–1699.

[15] Martinez, A., Palumbo, S., & Todd, B. D. (2019). Bioinspiration for Anisotropic Load Transfer at Soil–Structure Interfaces. Journal of Geotechnical and Geoenvironmental Engineering, 145(10), 1–14,. doi:10.1061/(asce)gt.1943-5606.0002138.

[16] Martinez, A., Zamora, F., & Wilson, D. (2024). Field Evaluation of the Installation and Pullout of Snakeskin-Inspired Anchorage Elements. Journal of Geotechnical and Geoenvironmental Engineering, 150(8), 04024068. doi:10.1061/jggefk.gteng-12311.

[17] Zhong, W., Liu, H., Wang, Q., Zhang, W., Li, Y., Ding, X., & Chen, L. (2021). Investigation of the penetration characteristics of snake skin-inspired pile using DEM. Acta Geotechnica, 16(6), 1849–1865. doi:10.1007/s11440-020-01132-2.

[18] O'Hara, K. B., & Martinez, A. (2022). Shaft and Base Capacity of Snakeskin-Inspired Piles from Centrifuge Pile Tests. Geo-Congress 2022, 170–180. doi:10.1061/9780784484029.016.

[19] Prandtl, L. (1918). Airfoil Theory—Communication I. Proceedings of the Royal Society of Göttingen, Mathematical-Physical Class, 451-477.

[20] Reissner, H. (1924). Regarding the earth pressure problem. Proceedings of the 1st international conference for applied mechanics, Delft, Netherlands. (In German).

[21] OuYang, H., Dai, G., & Gong, W. (2024). Analysis of influencing factors of penetration mechanism and vertical bearing characteristics of monopile in calcareous sand: Laboratory model testing and in-situ testing. Soil Dynamics and Earthquake Engineering, 180, 108577. doi:10.1016/j.soildyn.2024.108577.

[22] Zhang, L. (2024). Experimental Investigation of Vertical and Lateral Bearing Behaviors of Single Piles. Soil Mechanics and Foundation Engineering, 61(3), 239–247. doi:10.1007/s11204-024-09968-6.

[23] Maralapalle, V. C., Nadaf, M. B., Dutta, S., Zende, A. A., Mishra, S. S., & Charhate, S. (2023). Load-settlement and skin friction behaviour of piles in dry sand: experimental and numerical study. Sādhanā, 49(1), 4. doi:10.1007/s12046-023-02362-2.

[24] Qin, H., Zhao, X., & Li, S. (2021). Experiment study on bearing capacity of large-diameter long pile in large thickness backfill loess site. Proc.SPIE, 58. doi:10.1117/12.2619758.

[25] Terzaghi, K. (1943). Theoretical soil mechanics. Wiley, Hoboken, United States. doi:10.1002/9780470172766.

[26] Liang, C., & Liu, R. (2021). Calculation method for the vertical bearing capacity of a riser-surface casing composite pile. Ships and Offshore Structures, 16(S2), 66–76. doi:10.1080/17445302.2020.1861711.

[27] Shulyatyev, O. A., & Shulyatyev, S. O. (2023). Influence of pile foundation technology on the skin friction. Smart Geotechnics for Smart Societies, 2100–2108. doi:10.1201/9781003299127-321.

[28] Meyerhof, G. G. (1951). The Ultimate Bearing Capacity of Foundations. Géotechnique, 2(4), 301–332. doi:10.1680/geot.1951.2.4.301.

[29] Vesic, A. B. (1963). Bearing capacity of deep foundations in sand. Highway Research Record, (39), 112-153.

[30] Lee, J. H., & Salgado, R. (1999). Determination of Pile Base Resistance in Sands. Journal of Geotechnical and Geoenvironmental Engineering, 125(8), 673–683. doi:10.1061/(asce)1090-0241(1999)125:8(673).

[31] Hataf, N., & Shafaghat, A. (2015). Optimizing the Bearing Capacity of Tapered Piles in Realistic Scale Using 3D Finite Element Method. Geotechnical and Geological Engineering, 33(6), 1465–1473. doi:10.1007/s10706-015-9912-6.

[32] Moon, J. S., & Lee, S. (2016). Static skin friction behavior of a single micropile in sand. KSCE Journal of Civil Engineering, 20(5), 1793–1805. doi:10.1007/s12205-016-0918-2.

[33] Martinez, A., & Frost, J. D. (2018). Undrained Behavior of Sand–Structure Interfaces Subjected to Cyclic Torsional Shearing. Journal of Geotechnical and Geoenvironmental Engineering, 144(9), 1–13. doi:10.1061/(asce)gt.1943-5606.0001942.

[34] Wang, H., Wang, L. Z., Hong, Y., He, B., & Zhu, R. H. (2020). Quantifying the influence of pile diameter on the load transfer curves of laterally loaded monopile in sand. Applied Ocean Research, 101. doi:10.1016/j.apor.2020.102196.

[35] Abellan-Garcia, J., Abbas, Y. M., Khan, M. I., & Pellicer-Martínez, F. (2024). ANOVA-guided assessment of waste glass and limestone powder influence on ultra-high-performance concrete properties. Case Studies in Construction Materials, 20. doi:10.1016/j.cscm.2024.e03231.

[36] Megdouli, K., Gholizadeh, T., Tashtoush, B., Cinnella, P., & Skorek-Osikowska, A. (2024). Optimization of carbon dioxide ejector expansion transcritical refrigeration system with ANOVA and NSGA-II. International Journal of Refrigeration, 158, 173–189. doi:10.1016/j.ijrefrig.2023.11.012.

[37] Kumar, P., Almeida, F., AR, A., & Al-Mdallal, Q. (2025). Construction of optimised theoretical model using ANOVA -Taguchi methodology for transient flow of Carreau nanofluid through microchannel prone to radiation. Alexandria Engineering Journal, 112, 411–423. doi:10.1016/j.aej.2024.10.111.

[38] Ermergen, T., & Taylan, F. (2024). Investigation of DOE model analyses for open atmosphere laser polishing of additively manufactured Ti-6Al-4V samples by using ANOVA. Optics and Laser Technology, 168. doi:10.1016/j.optlastec.2023.109832.

[39] Gayathri, V. L., Vangla, P., & Riya, A. (2022). Effect of snakeskin-inspired patterns on the shear response of soil-continuum interfaces. International Journal of Geotechnical Engineering, 16(6), 759-775. doi:10.1080/19386362.2022.2066049.

[40] O'Hara, K. B., & Martinez, A. (2020). Effects of Asperity Height on Monotonic and Cyclic Interface Behavior of Bioinspired Surfaces under Constant Normal Stiffness Conditions. American Society of Civil Engineers (ASCE), 243–252. doi:10.1061/9780784482834.027.

[41] Song, J., Huang, H., Wang, X., & Shi, W. (2023). Status and prospects of surface texturing: Design, manufacturing and applications. Surface Science and Technology, 1(1), 21. doi:10.1007/s44251-023-00022-5.

[42] Sharafutdinov, V. A. T. (2023). A Radon-type transform related to the Euler equations for an ideal fluid. Siberian Electronic Mathematical News, 20(2), 880–912. doi:10.33048/semi.2023.020.054.

[43] Lee, S. H., Nawaz, M. N., & Chong, S. H. (2023). Estimation of interface frictional anisotropy between sand and snakeskin-inspired surfaces. Scientific Reports, 13(1), 3975. doi:10.1038/s41598-023-31047-3.

[44] Stutz, H. H., & Martinez, A. (2021). Directionally dependent strength and dilatancy behavior of soil–structure interfaces. Acta Geotechnica, 16(9), 2805–2820. doi:10.1007/s11440-021-01199-5.

[45] Han, F., Ganju, E., Salgado, R., & Prezzi, M. (2018). Effects of Interface Roughness, Particle Geometry, and Gradation on the Sand–Steel Interface Friction Angle. Journal of Geotechnical and Geoenvironmental Engineering, 144(12), 04018096. doi:10.1061/(asce)gt.1943-5606.0001990.

[46] Nawaz, M. N., Lee, S. H., Chong, S. H., & Ku, T. (2024). Interface frictional anisotropy of dilative sand. Scientific Reports, 14(1), 6166. doi:10.1038/s41598-024-56621-1.

[47] Chen, L., Zhang, Y., Cui, Y., Wang, J., & Wang, M. (2022). Effects of Snake-Bioinspired Surface Texture on the Finger-Sealing Performance under Varied Working Conditions. Machines, 10(7), 569. doi:10.3390/machines10070569.

[48] Duffy, K., Gavin, K., Korff, M., de Lange, D., & Roubos, A. (2024). Influence of Installation Method on the Axial Capacity of Piles in Very Dense Sand. Journal of Geotechnical and Geoenvironmental Engineering, 150(6), 04024043. doi:10.1061/jggefk.gteng-12026.

[49] Lehane, B. M., Schneider, J. A., & Xu, X. (2007). Development of the UWA-05 Design Method for Open and Closed Ended Driven Piles in Siliceous Sand. American Society of Civil Engineers (ASCE), 1–10. doi:10.1061/40902(221)12.

[50] Guo, Y., Wang, C., Bouazza, A., Kong, G., & Ding, X. (2025). Thermal performance of pipe-type energy piles with open-ended heat exchange tubes. Applied Thermal Engineering, 258. doi:10.1016/j.applthermaleng.2024.124573.

[51] Wang, J., Dove, J. E., & Gutierrez, M. S. (2007). Anisotropy-Based Failure Criterion for Interphase Systems. Journal of Geotechnical and Geoenvironmental Engineering, 133(5), 599–608. doi:10.1061/(asce)1090-0241(2007)133:5(599).

[52] Fang, J., Zhao, Y., Feng, S., Chen, H., & Zhou, X. (2024). Thermo-hydro-mechanical behavior of soft soils beneath energy shallow foundations subjected to thermal and mechanical loads. Computers and Geotechnics, 176. doi:10.1016/j.compgeo.2024.106790.

[53] Huang, L., & Martinez, A. (2021). Load Transfer Anisotropy at Snakeskin-Inspired Clay-Structure Interfaces. IFCEE 2021, 119–129. doi:10.1061/9780784483428.013.

[54] Zhang, N., Chen, Y., Martinez, A., & Fuentes, R. (2023). A Bioinspired Self-Burrowing Probe in Shallow Granular Materials. Journal of Geotechnical and Geoenvironmental Engineering, 149(9), 04023073. doi:10.1061/jggefk.gteng-11507.